
This is an electronic reprint of the original article.
This reprint may differ from the original in pagination and typographic detail.

Xu, Donghan; Zhang, Cuijuan; Li, Yongdan

Ferrocene/naphthalimide bi-redox molecule for enhancing the cycling stability of symmetric nonaqueous redox flow battery

Published in:
Journal of Power Sources

DOI:
[10.1016/j.jpowsour.2024.234368](https://doi.org/10.1016/j.jpowsour.2024.234368)

Published: 15/05/2024

Document Version
Publisher's PDF, also known as Version of record

Published under the following license:
CC BY

Please cite the original version:
Xu, D., Zhang, C., & Li, Y. (2024). Ferrocene/naphthalimide bi-redox molecule for enhancing the cycling stability of symmetric nonaqueous redox flow battery. *Journal of Power Sources*, 602, Article 234368.
<https://doi.org/10.1016/j.jpowsour.2024.234368>

This material is protected by copyright and other intellectual property rights, and duplication or sale of all or part of any of the repository collections is not permitted, except that material may be duplicated by you for your research use or educational purposes in electronic or print form. You must obtain permission for any other use. Electronic or print copies may not be offered, whether for sale or otherwise to anyone who is not an authorised user.



Ferrocene/naphthalimide bi-redox molecule for enhancing the cycling stability of symmetric nonaqueous redox flow battery

Donghan Xu^{a,b}, Cuijuan Zhang^{a,b,**}, Yongdan Li^{a,b,c,*}

^a State Key Laboratory of Chemical Engineering, Tianjin Key Laboratory of Applied Catalysis Science and Technology, School of Chemical Engineering and Technology, Tianjin University, Tianjin, 300072, China

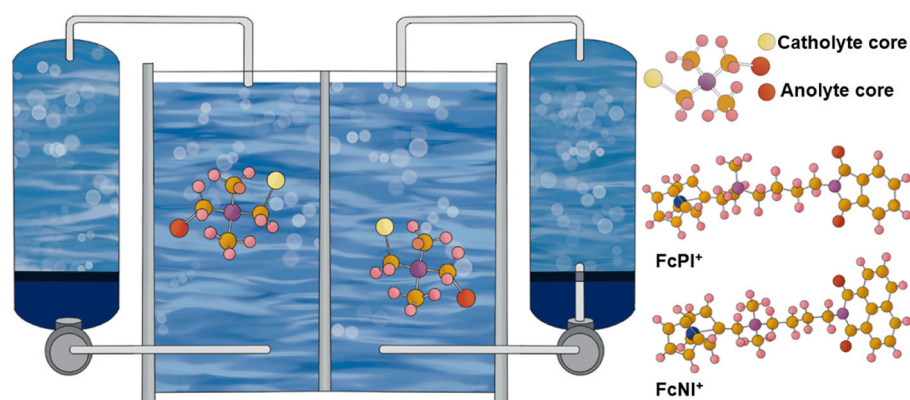
^b Collaborative Innovation Center of Chemical Science and Engineering (Tianjin), Tianjin, 300072, China

^c Department of Chemical and Metallurgical Engineering, School of Chemical Engineering, Aalto University, Kemistintie 1, Espoo, P.O. Box 16100, FI-00076, Aalto, Finland

HIGHLIGHTS

- A strategy is applied to construct ionic bipolar ROMs based on nucleophilic substitution.
- The FcNI-TFSI based NARFBs exhibit improved cycling stability with N_{50} of 233 at 0.1 M.
- Capacity diving phenomenon is observed in the high-concentration battery.
- The reasons for sudden accelerated capacity are explored.

GRAPHICAL ABSTRACT



ARTICLE INFO

Keywords:

Electrochemical energy storage
Symmetric nonaqueous redox flow battery
Bipolar redox-active organic molecules
Ferrocene
Naphthalimide
Nucleophilic substitution

ABSTRACT

Derived from N-(ferrocenylmethyl)-N-(butylphthalimide)-N,N-dimethylammonium bis(trifluoromethanesulfonyl)imide (FcPI-TFSI), ferrocene/naphthalimide (FcNI-TFSI) based ionic bipolar redox-active organic molecule is constructed via nucleophilic substitution between amines and halogenated hydrocarbons. Due to the elevated delocalized negative charge density in the radical anion, the FcNI-TFSI based nonaqueous redox flow batteries (NARFBs) exhibits substantially improved cycling stability; 764 and 233 cycles are successfully performed before 50% of the initial discharge capacity is lost at 0.01 M and 0.1 M, respectively, whereas 82 cycles for FcPI-TFSI at 0.01 M. Similar to capacity diving phenomenon in lithium-ion batteries, sudden accelerated

* Corresponding author. State Key Laboratory of Chemical Engineering, Tianjin Key Laboratory of Applied Catalysis Science and Technology, School of Chemical Engineering and Technology, Tianjin University, Tianjin, 300072, China.

** Corresponding author. State Key Laboratory of Chemical Engineering, Tianjin Key Laboratory of Applied Catalysis Science and Technology, School of Chemical Engineering and Technology, Tianjin University, Tianjin, 300072, China.

E-mail addresses: cjzhang@tju.edu.cn (C. Zhang), yongdan.li@aalto.fi (Y. Li).

<https://doi.org/10.1016/j.jpowsour.2024.234368>

Received 7 November 2023; Received in revised form 9 March 2024; Accepted 13 March 2024

Available online 25 March 2024

0378-7753/© 2024 The Authors. Published by Elsevier B.V. This is an open access article under the CC BY license (<http://creativecommons.org/licenses/by/4.0/>).

capacity loss is observed in the high-concentration battery. The possible degradation mechanism is discussed, involving crossover issue and parasitic reactions.

1. Introduction

Large-scale energy storage technology, as an integral part of renewable power plants, provides a feasible solution for integrating renewable energy, maintaining the balance between supply and demand of power generation, and enhancing the security and resilience of grid modernization [1,2]. The redox flow battery (RFB) is widely considered to be one of the most promising candidates for practical application. The unique feature of spatial separation between electrolyte and electrode offers high safety and flexibility in decoupled energy and power units [3, 4]. Among the various RFB systems, the state-of-the-art all-vanadium RFBs (VRFBs) have made continuous progress toward commercialization [5,6]. The system produces an open-circuit voltage (OCV) of 1.25 V involving the charge transfer of $\text{VO}^{2+}/\text{VO}_2^+$ and $\text{V}^{3+}/\text{V}^{2+}$ redox couples. The same V element at cathode and anode sides alleviates the crossover issue between two half-cell electrolytes through the membrane. However, VRFBs suffer from corrosive electrolytes, high cost of vanadium elements, and limited energy density due to low voltages [5,6], which hinder their further market penetration.

Non-aqueous RFBs (NARFBs) utilizing organic solvents have recently harvested burgeoning interest as alternatives due to broader potential windows and the potentially higher energy density [7]. Conventional NARFBs are always beset by crossover due to the electrolyte difference between catholyte and anolyte, which will induce self-discharge and complex parasitic reactions of mixed electrolytes, ultimately leading to low Coulombic efficiency (CE) and irreversible capacity loss [8,9]. Emulating VRFBs, symmetric NARFBs with the same bipolar redox-active organic molecules (ROMs) at both half-cell sides have shown promise to alleviate the crossover issue. Several bipolar conjugated species which can undergo multiple redox reactions have been developed, diaminoanthraquinone [9,10], boron-dipyrromethene dye [11], nitronyl nitroxides [12,13], verdazyl radicals [14], thianthrene-quinone [15], diphenylanthracene [16], and thianthrene-quinone [17], just to name a few. Some NARFBs based on the bipolar conjugated species conjugated bipolar systems with OCV of up to 3 V. However, these systems suffer from poor cycling stability in flow cells. A facile solution is to construct artificial bipolar ROMs by linking the catholyte and anolyte moieties with electrochemically inactive scaffolds, e.g., N-ferrocenylphthalimide (FcNI) [18,19], functionalized fullerene derivatives [20], 1-(ferrocenylmethyl-amino)-anthraquinone (FcMeAAQ) [21], and 1-(2-(4-methoxy-2,5-dimethylphenoxy) ethyl)-1'-methyl-[4,4'-bipyridine]-1,1'-dium hexafluorophosphate (VIODAMB) [22]. Nevertheless, the large molecular size results in decreased solubility.

Previously, we constructed bipolar ROM by introducing tetraalkylammonium ionic moiety between different catholyte and anolyte redox cores, yielding N-(ferrocenylmethyl)-N-(butylphthalimide)-N,N-dimethylammonium bis(trifluoromethane-sulfonyl)imide (FcPI-TFSI). Such ionic compound holds promising prospects due to the high solubility benefited from the polar tetraalkylammonium ionic moiety. The related NARFBs exhibited fairly stable cycling (84.1% discharge capacity retention over 50 cycles at 7.5 mA cm^{-2} , 0.01 M) [23]. There is still great room to improve. Herein, to further promote the cycle stability, ferrocene/naphthalimide (FcNI-TFSI) is designed via similar nucleophilic substitution with increased conjugated π -bond systems (Scheme 1). The resultant battery exhibits substantially improved cycling stability, i.e., 764 cycles are successfully performed before 50% of the initial discharge capacity is lost whereas 82 cycles for FcPI-TFSI at 10 mA cm^{-2} , 0.01 M.

2. Experimental

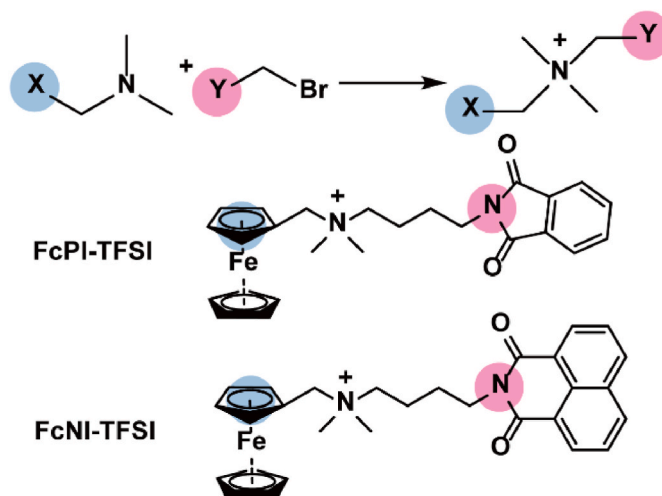
2.1. Materials

1,8-naphthalimide (Meryer, 98%), 1,4-dibromobutane (HEOWNS, 98%), (dimethylaminomethyl)ferrocene (Adamas, 97%), N-(4-bromobutyl)phthalimide (HEOWNS, 97%), lithium bis(trifluoromethylsulfonyl)imide (LiTFSI) (Meryer, 99.5%), tetrahydrofuran (THF) (MACKLIN, 99%), acetonitrile (MeCN) (Sigma-Aldrich, 99.9%), N,N-dimethylformamide (DMF) (Aladdin, 99.9%), propylene carbonate (PC) (Aladdin, 99%), ethyl acetate (Jiangtian, 99%), n-hexane (Jiangtian, 98%), dichloromethane (Jiangtian, 99%), methanol (Concord, 99.9%), ethanol (Jiangtian, 99.7%), sodium chloride (Aladdin, 99.5%), sodium sulfate (Bide, 99.03%), and silver nitrate (Aladdin, 99.8%) were purchased and used. Electrolyte solvents used for flow battery tests were further dried with 3 \AA molecular sieves (Acros Organics) at $260 \text{ }^\circ\text{C}$ for 24 h. Tetraethylammonium bis(trifluoromethylsulfonyl)imide (TEATFSI) and FcPI-TFSI were synthesized according to the reported procedures [23,24].

2.2. Synthesis of redox-active materials

Synthesis of N-(4-bromobutyl)naphthalimide: N-(4-bromobutyl)naphthalimide was synthesized by modifying the reported procedure [25]. To a solution of 1,8-naphthalimide (4 g, 20 mmol) in DMF (140 mL), 1,4-dibromobutane (17.28 g, 80 mmol), potassium carbonate (11.05 g, 80 mmol) were added. The mixture was stirred at room temperature for 24 h and partitioned between saturated aqueous sodium chloride and ethyl acetate. The aqueous phase was extracted with ethyl acetate three times and the combined organic phase were washed with saturated aqueous sodium chloride three times to remove DMF solvent. The organic phase was dried over sodium sulfate and evaporated under vacuum to obtain the crude product, which was further purified by column chromatography (ethyl acetate/n-hexane) to obtain pure N-(4-bromobutyl)naphthalimide. The white product was dried under vacuum for 24 h and obtained at 4.80 g, 72% yield.

Synthesis of FcNI-TFSI: N-(4-bromobutyl)naphthalimide (5 g, 15



Scheme 1. Nucleophilic substitution between amines and halogenated hydrocarbons and structural formulas of two targeted bipolar ROMs. X and Y can be different catholyte and anolyte redox cores, and the tetraalkylammonium ionic moiety is beneficial to promote the dissolution of bipolar ROMs in polar solvents.

mmol) was reacted with (dimethylaminomethyl)ferrocene (4.38 g, 18 mmol) in THF (50 mL) under an argon atmosphere (Liufang, 99.999%). The mixture was stirred at 55 °C for 24 h, filtered, washed with ether, and dried under vacuum to obtain FcNI-Br. FcNI-Br was dissolved in 500 mL deionized water at 80 °C, followed by the addition of aqueous LiTFSI (5.74 g, 20 mmol). The mixture was stirred for 2 h under an argon atmosphere, filtered, and dried under vacuum. The crude product was purified by column chromatography (dichloromethane/methanol). The orange product was dried under vacuum for 24 h and obtained at 9.51 g, 75% yield.

2.3. Characterization

Cyclic voltammetry (CV) tests: The CV tests were performed using a three-electrode configuration under argon atmosphere on a VersaSTAT3 electrochemical workstation (Princeton Applied Research, USA). A glassy carbon (6 mm in diameter), graphite plate (5.24 cm²), and Ag/Ag⁺ (0.5 M AgNO₃/MeCN) were employed as the working, counter, and reference electrodes, respectively. The electrolytes were purged with argon before CV tests. The diffusion coefficients (*D*) and kinetic rate constants (*k₀*) of redox-active materials were calculated according to the modified Randles-Sevcik equation and Nicholson method, respectively [26,27].

Solubility and conductivity measurement: The solubilities of bipolar redox-active organic molecules in 1.0 M TEATFSI/DMF were measured by ultraviolet–visible (UV–vis) spectrometer (PerkinElmer, Lambda 750, USA). The standard curves were obtained through a range of prepared solutions with different concentration of bipolar redox-active organic molecules. The saturated solutions were prepared in 1 mL 1.0 M TEATFSI/DMF and the supernatant was diluted and subjected to ultraviolet–visible (UV–vis) tests, and the solubilities were extrapolated based on the calculated standard curves. The molar ion conductivities of two compounds were measured by conductivity meter (INESA DDS-307A, China) with a concentration range of 2.5–12.5 mM in DMF at room temperature.

Flow battery tests: A sandwich-structured battery with graphite felts (4 cm², Morgan WDF-5) as electrodes and Daramic-250 (250 μm thick, pore size 150 nm) as separator was carried out by LAND battery test instrument (Wuhan LAND Electronic Co. Ltd., China) in the argon-filled glove box. Graphite felts and commercial separator were ultrasonically with ethanol cleaned and dried under vacuum at 70 °C for 24 h. The electrolytes (5 mL on each side) were circulated between cells and storage tanks by two peristaltic pumps (BT100-1L, Longer Precision Pump Co., Ltd., China) at a flow rate of 30 mL min⁻¹. The flow cells were circulated for 10 min and activated for 5 cycles prior to the battery test. Current-voltage polarization curve was measured through linear sweep voltammetry (LSV) at 100 mV s⁻¹ after the battery was charged to certain state of charge (SOC). The cycled electrolyte and precipitates were collected and subjected to liquid chromatography-high resolution mass spectrometry (LC-HRMS) analysis.

2.4. Computation methods

The quantum chemical parameters were obtained using the density functional theory (DFT) with the Gaussian 09 package [28]. The B3LYP density functional method with the D3(BJ) dispersion correction was employed in this work to carry out all the computations. The 6-31+G(d) basis set was used for the small atoms and SDD for Fe atoms. All structures have been optimized considering solvent effects using the PCM model for DMF. Vibrational frequency analyses at the same level of theory were performed on all optimized structures to characterize stationary points as local minima.

3. Results and discussion

FcNI-TFSI was synthesized through nucleophilic substitution of

redox-core-derived amine and halogenated hydrocarbon and subsequent ion exchange reaction of Br⁻ with TFSI⁻, and the corresponding ¹H NMR spectrum is shown in Fig. S1. The electrochemical properties were evaluated through CV tests (Fig. 1a). All show two pairs of electrochemically reversible redox peaks; the half-wave potential is 0.17 V vs. Ag/Ag⁺ for Fc moiety, -1.87 V for phthalimide (PI) moiety, and -1.72 V for naphthalimide (NI) moiety, resulting in OCV of 2.04 V for FcPI-TFSI and 1.89 V for FcNI-TFSI. The DFT calculation was performed to further evaluate the redox properties and electronic structures of two compounds (Fig. 1b). The oxidation and reduction potentials are dominated by the highest occupied molecular orbital (HOMO) energies and the lowest unoccupied molecular orbital (LUMO) energies, respectively. The lower LUMO energy for FcNI-TFSI accounts for the more positive reduction potential. FcPI-TFSI and FcNI-TFSI show the same oxidation potential and similar electron density distribution in Fc moieties of HOMO states. It indicates that almost no interaction exists in the redox cores at two sides, which once again proves the universality of the method of constructing bipolar ROMs.

The CV test was performed to explore the mass- and charge-transfer kinetics (Fig. S2). The ratio between cathodic and anodic peak current of all compounds is almost unity. The peak currents exhibit a linear relationship with the square root of the scan rate, which indicates a quasi-reversible diffusion-controlled process [29]. The *D* and *k₀* values were calculated according to the modified Randles-Sevcik equation and the Nicholson method, respectively (Table S1) [26,27]. Despite the increase in the molecular size, the kinetic parameters of the two compounds are higher than most bipolar ROMs, and even comparable with the conventional unipolar ROMs. The *D* and *k₀* values of conventional bipolar ROMs are in the order of 10⁻⁶ cm² s⁻¹ and 10⁻³ cm s⁻¹, respectively [21,30–32].

The solubilities of the compounds in 1.0 M TFATFSI/DMF evaluated by UV–vis spectroscopy are 1.86 M for FcPI-TFSI and 0.79 M for FcNI-TFSI (Fig. S3). Benefiting from the preferential solvation of the polar tetraalkylammonium ionic moiety, the targeted compounds exhibit solubility of comparable with and even superior to the reported, e.g., 2.6 M for 2-phenyl-4,4,5,5-tetramethylimidazoline-1-oxyl-3-oxide in MeCN [12], 0.2 M for boron-dipyrromethene dye in MeCN [11], 0.02 M for diaminoanthraquinones in MeCN [9], 0.3 M for FcPI in 1.0 M tetrabutylammonium tetrafluoroborate (TBABF₄)/1,3-dioxolane (1,3-DL) [18], 0.81 M for N-(α-ferrocenyl) ethylphthalimide in 1.0 M TBABF₄/1,3-DL [19], 0.122 M for 1,4-bis((2-(2-(2-methoxyethoxy)ethoxy)ethyl) amino) anthracene-9,10-dione in 1,2-dimethoxyethane (DME) [10], 0.017 M for FcMeAAQ in DMF [21], and 0.53 M for VIODAMB in 1.0 M TEATFSI/DME [22]. Furthermore, the inherent high ion conductivity of the compounds is another advantage, which was measured by conductivity meter at a concentration from 2.5 mM to 12.5 mM in DMF. The conductivity shows a linear relationship with the concentration (Fig. S4) and the slope is the molar ion conductivity, which is 65.0 and 62.3 S cm² mol⁻¹ for FcPI-TFSI and FcNI-TFSI, respectively, which rivals the supporting electrolyte (85.9 S cm² mol⁻¹ for TEATFSI) [23]. The similar molar conductivity may be due to the same TFSI⁻, which dominates the ion conductivity. The high inherent ion conductivity is beneficial for the rate capability.

Cycling stability of the redox-active electrolyte is one of important performance metrics, which directly determine the lifetime and cost of NARFBs. Previously, it was characterized by the capacity retention rate after a certain number of cycles [33–35]. Such indicator lacks uniformity due to the different cycle number of the batteries. Here, we evaluate the cycling stability of FcPI-TFSI and FcNI-TFSI based electrolytes with the descriptor of N₅₀, the cycle number before 50% of the initial discharge capacity is lost, which was proposed by Silcox et al. [36]. The galvanostatic cycling test was performed in the flow cells with 0.01 M bipolar ROMs in 1.0 M TEATFSI/DMF as both catholyte and anolyte and Daramic-250 as the membrane at 100% SOC and 10 mA cm⁻² (Fig. 2a). The FcPI-TSI based flow cell exhibits stable cycling initially with the discharge capacity retention of 81.1% over 50 cycles but rapid capacity

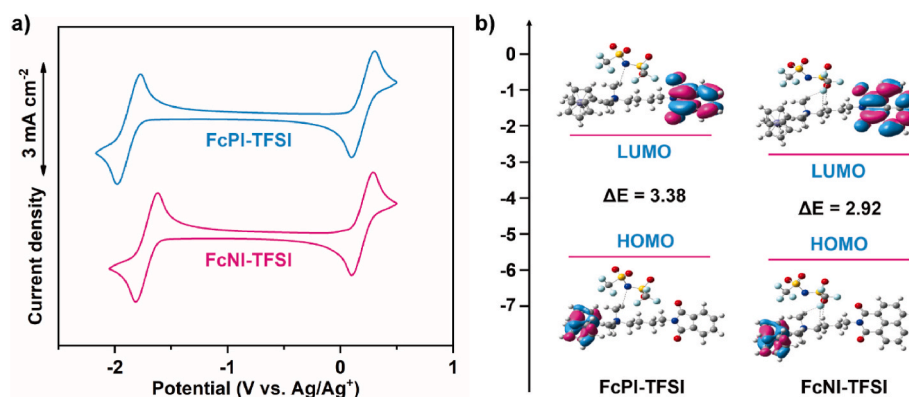


Fig. 1. (a) CV curves of 0.01 M bipolar ROMs in 0.1 M TEATFSI/DMF at a scan rate of 100 mV s^{-1} . (b) DFT calculation results of the molecular orbital energy levels of two bipolar ROMs.

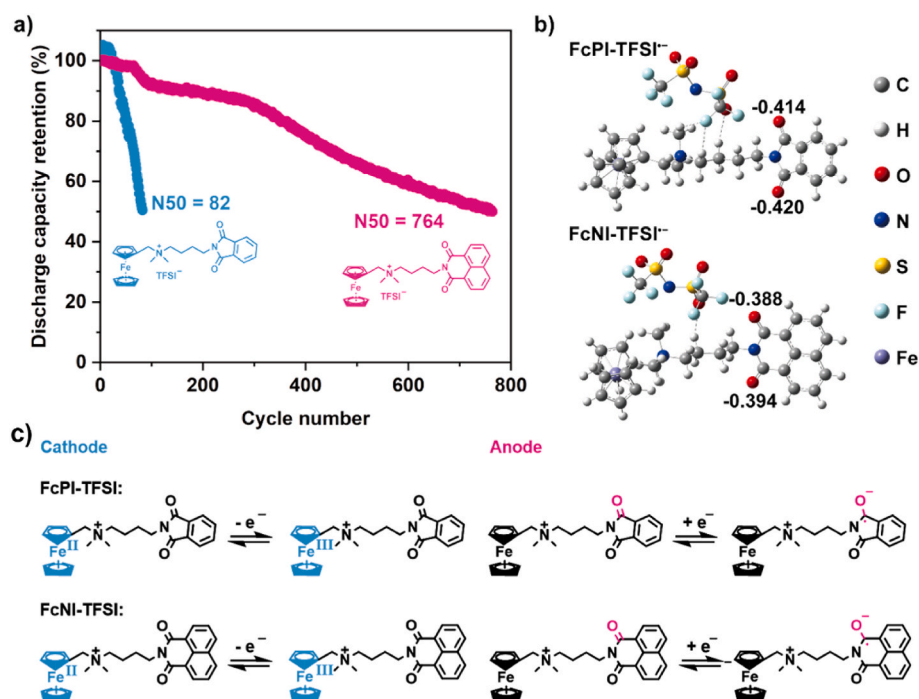


Fig. 2. (a) Discharge capacity of the flow cells based on 0.01 M bipolar ROM (FcPI-TFSI or FcNI-TFSI) in 1.0 M TEATFSI/DMF at 10 mA cm^{-2} . (b) The optimized structure of FcPI-TFSI $^{\bullet-}$ and FcNI-TFSI $^{\bullet-}$ and Hirshfeld charge densities at the redox-active sites. (c) Schematic of redox reactions of FcPI-TFSI and FcNI-TFSI.

loss subsequently, with N_{50} of 82. The CV curve for 100 cycled-FcPI-TFSI deteriorates with reduced reversibility of the redox peaks at the Ph moiety. In addition, a new redox couple is observed at 0 V vs. Ag/Ag^+ , which can be assigned to the redox of pristine Fc (Fig. S5) [37]. In sharp contrast, its FcNI-TSI counterpart-based flow cell exhibits significantly improved cycling stability, with N_{50} of 764. As for capacity loss, one main reason is the parasitic reaction of ROMs, especially in the free radical state, which usually exhibits chemical instability [38]. Fig. 2b and c shows the Hirshfeld charge densities at the redox-active sites using the DFT method and schematic of redox reactions of FcPI-TFSI and FcNI-TFSI, respectively. The electrode reactions of FcPI-TFSI and FcNI-TFSI involve radical anion at the anode side [23,39]. The increased conjugated π -bond systems of FcNI-TFSI $^{\bullet-}$ boosts the delocalization of negative charges and decreases the charge on the oxygen atom of the carbonyl group, leading to alleviated electrophilic attack by cations and electron-deficient groups from the electrolyte and thus significantly enhanced stability [40]. The result indicates that constructing extended π -conjugated system is an effective method to improve the stability of

ROMs [33]. It is worth noting that although FcNI-TFSI based battery delivers higher cycling stability, a lower OCV and energy density will cause a slight decrease, which is a tradeoff.

Encouraged by the significantly improved stability of FcNI-TFSI, a higher concentration flow cell with 0.1 M FcNI-TFSI in 1.0 M TEATFSI/DMF was assembled to examine the cycling stability and rate capability. The kinematic viscosity is $0.012 \text{ cm}^2 \text{ s}^{-1}$ on capillary viscometer. Based on the decay rate of the discharge capacity, the charge/discharge curve can be divided into three stages (Fig. 3a and Fig. S6). During the first stage (1st-25th cycles), the capacity decays rapidly. The respective maximum charge and discharge capacity are 2.32 and 2.20 Ah L^{-1} , corresponding to a maximum charge energy density of 5.24 Wh L^{-1} . The 25-cycled CV curves show the same profile with the fresh electrolyte, indicating that the parasitic reaction of ROM is not the main reason for the capacity decay. Even for symmetric batteries, crossover is still unavoidable due to the concentration difference between different charged species during cycling, which is exacerbated with increased concentration and the charge/discharge duration per cycle. Accordingly,

crossover should be mainly responsible for the capacity decay at this stage [18,21]. During the following second stage (25th–140th cycle), the diffusion across membrane probably reaches equilibrium and thus the influence of crossover becomes weak. The CV analysis suggests that the electrolyte parasitic reactions can be neglected. Correspondingly, the capacity remains remarkably stable. During the third stage (beyond 140th cycle), however, the capacity decays quickly again. Sudden accelerated capacity loss is similar to capacity diving phenomenon commonly observed in lithium-ion batteries [41,42], which is worth researching. The cycled CV shows new oxidation peak at 0 V and reduction peak at -0.1 V, assigned to Fc moiety [37]. The capacity decay at this stage is resulted from the electrolyte parasitic reactions. The postmortem examination reveals small number of precipitates in the electrolyte. The HRMS of the cycled electrolyte and precipitates and the resultant proposed degradation pathway are shown in Fig. S7. The FcNI-TFSI molecule may undergo bond breakage between Fc moiety and quaternary ammonium. The major by-product in the cycled electrolyte displays molecular ion peak at $m/z = 297$, which is assigned to molecular fragment including NI moiety and amine. The major species in the precipitate with $m/z = 199$ is presumed to be fragmented methyl Fc moiety. The decreased solubility of fragmented Fc moiety results in solid precipitation, which is also confirmed by the new redox peaks in the CV curves after 250 cycles (Fig. 3a). The stability of Fc moiety can be further

improved by the extension of the methylene chain between Fc moiety and quaternary ammonium to establish + I inductive effect of the electron-donating functional group as reported [43–45], which will be carried out in the future. Nonetheless, the battery exhibits excellent cycling stability with N_{50} of 764 at 0.01 M and 233 at 0.1 M. It is superior to most reported symmetric NARFBs based on bipolar ROMs in terms of cycling stability [9–21], only somewhat inferior to the 1,2,4-benzotriazin-4-yl (Blatter) radicals based battery with 97% capacity retention over 50 cycles [46] and the phenothiazine/phthalimide bipolar molecule based battery with 68.6% capacity retention over 275 cycles and 5 cell polarity reversals [47].

The I–V polarization curve at 100% SOC (Fig. 3b) shows a peak power density of 83.4 mW cm^{-2} , which surpasses most reported metal coordination complexes based batteries, but slightly inferior to asymmetric battery based on unipolar ROM due to larger molecular size [21, 48,49]. Before the rate performance test, the battery was activated for several cycles in order to allow the test to fall into the second stage with constant discharge capacity. When the current density (j) increases from 10 to 50 mA cm^{-2} , CE increases from 90.6% to 98.7% (Fig. 3c) due to the reduced charge/discharge duration and self-discharge. However, due to the exacerbated polarization loss, the discharge capacity and voltage efficiency (VE) decrease from 2.56 Ah L^{-1} and 80.6% to 1.08 Ah L^{-1} and 22.7%, respectively. When j is reset to 10 mA cm^{-2} , the discharge

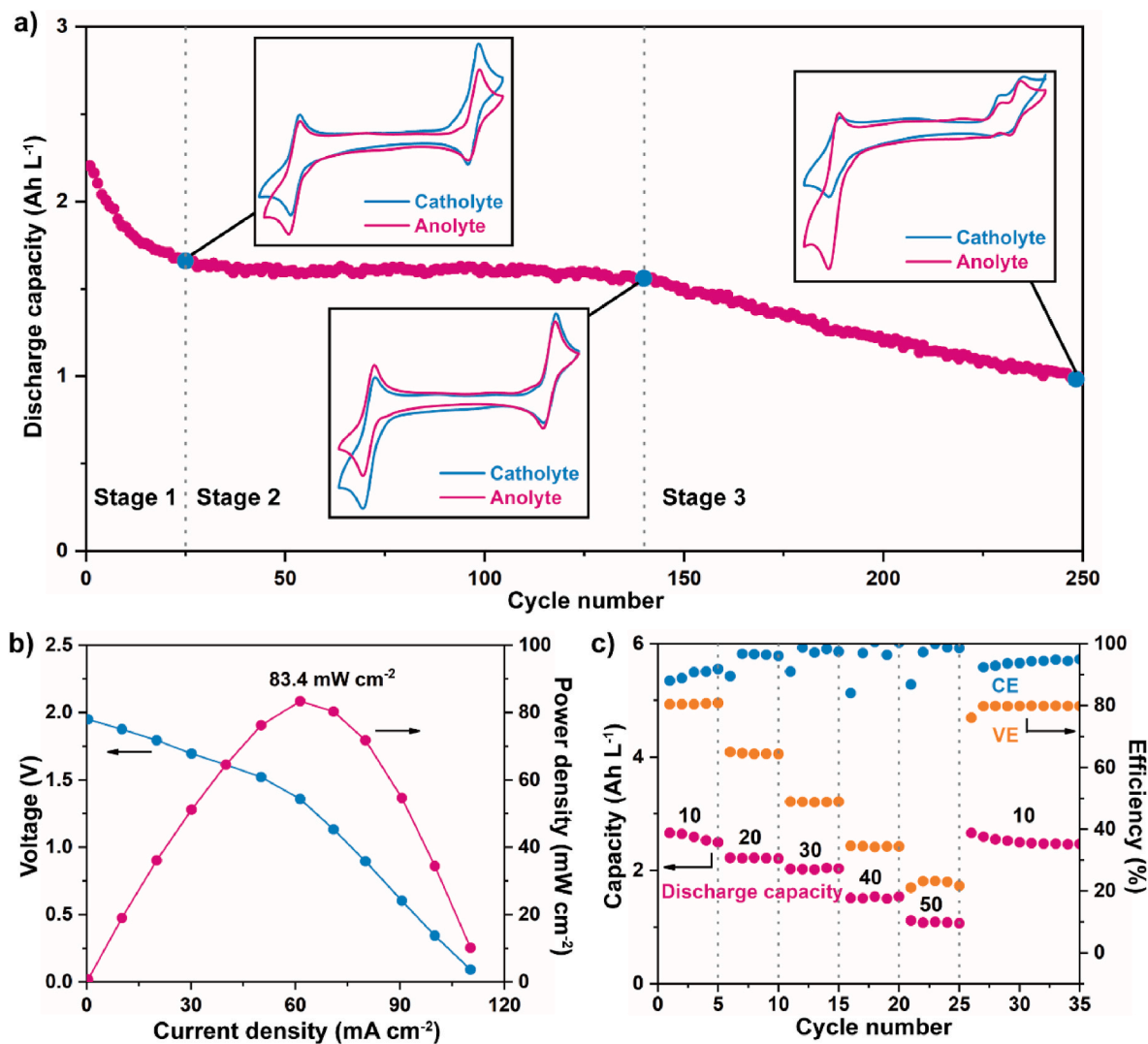


Fig. 3. (a) Discharge capacity of the flow cell based on 0.1 M FcNI-TFSI in 1.0 M TEATFSI/DMF at 40 mA cm^{-2} . Inset is the CV curves of the catholyte and anolyte after a specific cycle number. (b) Polarization curves of the battery at 100% SOC. (c) Rate performance from 10 to 50 mA cm^{-2} .

capacity of the battery recovers to the initial level, indicating the robustness of the flow cell with current fluctuations. Although the organic systems can provide a higher OCV, it is worth noting that the organic solvents are toxic and flammable.

4. Conclusions

In summary, we improved the electrochemical stability of the ionic bipolar ROMs though the increased conjugated π -bond system and decreased charge on the oxygen atom of the carbonyl group in the radical anion, as verified by DFT simulation. Benefited from the polar tetraalkylammonium ionic moiety, the FcNI-TFSI compound exhibits solubility of 0.79 M in 1.0 TEATFSI/DMF and inherent molar ion conductivity of $62.3 \text{ S cm}^2 \text{ mol}^{-1}$. The resulting NARFB based on FcNI-TFSI delivers a substantially enhanced cycling stability, with N_{50} of 764 cycles vs. 82 for FcPI-TFSI at 0.01 M and 223 at 0.1 M. Sudden accelerated capacity loss is observed after 140 cycles at 0.1 M. Possible parasitic reaction involving the bond breakage between Fc moiety and quaternary ammonium should be responsible for the diving phenomenon. Further improvement of the stability of Fc moiety can be done by establishing + I inductive effect of the electron-donating functional group.

CRedit authorship contribution statement

Donghan Xu: Writing – original draft, Methodology, Investigation, Formal analysis, Conceptualization. **Cuijuan Zhang:** Writing – review & editing, Supervision, Methodology, Conceptualization. **Yongdan Li:** Supervision, Resources, Funding acquisition.

Declaration of competing interest

The authors declare that they have no known competing financial interests or personal relationships that could have appeared to influence the work reported in this paper.

Data availability

Data will be made available on request.

Acknowledgements

The work was financially supported by the National Natural Science Foundation of China (21636007).

Appendix A. Supplementary data

Supplementary data to this article can be found online at <https://doi.org/10.1016/j.jpowsour.2024.234368>.

References

- [1] I. Hadjipaschalis, A. Poullikkas, V. Efthimiou, *Renew. Sust. Energ. Rev.* 13 (2009) 1513–1522.
- [2] B. Dunn, H. Kamath, J.M. Tarascon, *Science* 334 (2011) 928–935.
- [3] G.L. Soloveichik, *Chem. Rev.* 115 (2015) 11533–11558.
- [4] W. Wang, Q. Luo, B. Li, X. Wei, L. Li, Z. Yang, *Adv. Funct. Mater.* 23 (2013) 970–986.
- [5] C. Ding, H. Zhang, X. Li, T. Liu, F. Xing, *J. Phys. Chem. Lett.* 4 (2013) 1281–1294.
- [6] L. Li, S. Kim, W. Wang, M. Vijayakumar, Z. Nie, B. Chen, J. Zhang, G. Xia, J. Hu, G. Graff, J. Liu, Z. Yang, *Adv. Energy Mater.* 1 (2011) 394–400.
- [7] K. Gong, Q. Fang, S. Gu, S. Li, Y. Yan, *Energy Environ. Sci.* 8 (2015) 3515–3530.
- [8] J. Winsberg, C. Stolze, S. Muench, F. Liedl, M.D. Hager, U.S. Schubert, *ACS Energy Lett.* 1 (2016) 976–980.
- [9] R.A. Potash, J.R. McKone, S. Conte, H.D. Abruna, *J. Electrochem. Soc.* 163 (2016) A338–A344.
- [10] P. Geysens, Y. Li, I. Vankelecom, J. Franssaer, K. Binnemans, *ACS Sustainable Chem. Eng.* 8 (2020) 3832–3843.
- [11] A.M. Kosswattarachchi, A.E. Friedman, T.R. Cook, *ChemSusChem* 9 (2016) 3317–3323.
- [12] W. Duan, R.S. Vemuri, J.D. Milshtein, S. Laramie, R.D. Dmello, J. Huang, L. Zhang, D. Hu, M. Vijayakumar, W. Wang, J. Liu, R.M. Darling, L. Thompson, K. Smith, J. S. Moore, F.R. Brushett, X. Wei, *J. Mater. Chem. A* 4 (2016) 5448–5456.
- [13] T. Hagemann, J. Winsberg, B. Haupler, T. Janoschka, J.J. Gruber, A. Wild, U. S. Schubert, *NPG Asia Mater.* 9 (2017) e340.
- [14] G.D. Charlton, S.M. Barbon, J.B. Gilroy, C.A. Dyker, *J. Energy Chem.* 34 (2019) 52–56.
- [15] S.I. Etkind, J. Lopez, Y. Zhu, J.H. Fang, W.J. Ong, Y. Shao-Horn, T.M. Swager, *ACS Sustain. Chem. Eng.* 10 (2022) 11739–11750.
- [16] J.D. Saraidaridis, J.A. Suttill, C.W. Monroe, *J. Electrochem. Soc.* 167 (2020) 070517.
- [17] Y. Liu, G. Dai, Y. Chen, R. Wang, H. Li, X. Shi, X. Zhang, Y. Xu, Y. Zhao, *ACS Energy Lett.* 7 (2022) 1274–1283.
- [18] S. Hwang, H.S. Kim, J.H. Ryu, S.M. Oh, *J. Power Sources* 395 (2018) 60–65.
- [19] S. Hwang, H.S. Kim, J.H. Ryu, S.M. Oh, *J. Power Sources* 421 (2019) 1–5.
- [20] J. Friedl, M.A. Lebedeva, K. Porfyrakis, U. Stimming, T.W. Chamberlain, *J. Am. Chem. Soc.* 140 (2018) 401–405.
- [21] Y. Zhen, C. Zhang, J. Yuan, Y. Zhao, Y. Li, *J. Power Sources* 480 (2020) 229132.
- [22] B. Liu, C. Tang, F.K. Sheong, G. Jia, T. Zhao, *ACS Sustainable Chem. Eng.* 10 (2022) 613–621.
- [23] D. Xu, C. Zhang, Y. Zhen, Y. Li, *ACS Appl. Energy Mater.* 4 (2021) 8045–8051.
- [24] L. Timperman, P. Skowron, A. Boisset, H. Galiano, D. Lemordant, E. Frackowiak, F. Beguin, M. Anouti, *Phys. Chem. Chem. Phys.* 14 (2012) 8199–8207.
- [25] J. Ramchander, *Chem. Sci. Trans.* 5 (2016) 163–170.
- [26] A.J. Bard, L.R. Faulkner, *Electrochemical Methods: Fundamentals and Applications*, Wiley, 2001.
- [27] R.S. Nicholson, *Anal. Chem.* 37 (1965) 1351–1355.
- [28] M.J. Frisch, G.W. Trucks, H.B. Schlegel, et al., Gaussian 09, Gaussian, Inc., Wallingford CT, 2013.
- [29] T. Pajkossy, *Electrochem. Commun.* 90 (2018) 69–72.
- [30] G. Kwon, K. Lee, M.H. Lee, B. Lee, S. Lee, S.K. Jung, K. Ku, J. Kim, S.Y. Park, J. E. Kwon, K. Kang, *Chem* 5 (2019) 2642–2656.
- [31] D. Xu, C. Zhang, Y. Zhen, Y. Li, *ACS Appl. Mater. Interfaces* 13 (2021) 35579–35584.
- [32] D. Xu, C. Zhang, Y. Li, *Curr. Opin. Chem. Eng.* 37 (2022) 100851.
- [33] S. Ahn, J. Jang, J. Kang, M. Na, J. Seo, V. Singh, J.M. Joo, H.R. Byon, *ACS Energy Lett.* 6 (2021) 3390–3397.
- [34] L. Zhang, Y. Qian, R. Feng, Y. Ding, X. Zu, C. Zhang, X. Guo, W. Wang, G. Yu, *Nat. Commun.* 11 (2020) 3843.
- [35] B. Liu, C. Tang, C. Zhang, G. Jia, T. Zhao, *Chem. Mater.* 33 (2021) 978–986.
- [36] B. Silcox, J. Zhang, I.A. Shkrob, L. Thompson, L. Zhang, *J. Phys. Chem. C* 123 (2019) 16516–16524.
- [37] Y. Zhen, C. Zhang, J. Yuan, Y. Zhao, Y. Li, *J. Power Sources* 445 (2020) 227331.
- [38] X. Wei, W. Xu, J. Huang, L. Zhang, E. Walter, C. Lawrence, M. Vijayakumar, W. A. Henderson, T.B. Liu, L. Cosimbescu, B. Li, V. Sprenkle, W. Wang, *Angew. Chem. Int. Ed.* 54 (2015) 8684–8687.
- [39] D. Xu, C. Zhang, Y. Li, *Chem. Eng. J.* 439 (2022) 135766.
- [40] W. Duan, J. Huang, J.A. Kowalski, I.A. Shkrob, M. Vijayakumar, E. Walter, B. F. Pan, Z. Yang, J.D. Milshtein, B. Li, C. Liao, Z. Zhang, W. Wang, J. Liu, J.S. Moore, F.R. Brushett, L. Zhang, X. Wei, *ACS Energy Lett.* 2 (2017) 1156–1161.
- [41] Y. Wang, X. Chang, Z. Li, Y. Mei, Y. Zhang, L. Liu, K. Wang, H. Gu, L. Li, *Adv. Funct. Mater.* 33 (2023) 2208329.
- [42] S.F. Schuster, T. Bach, E. Fleder, J. Muller, M. Brand, G. Sextl, A. Jossen, *J. Energy Storage* 1 (2015) 44–53.
- [43] J. Luo, M. Hu, W. Wu, B. Yuan, T. Liu, *Energy Environ. Sci.* 15 (2022) 1315–1324.
- [44] E.S. Beh, D. De Porcellinis, R.L. Gracia, K.T. Xia, R.G. Gordon, M.J. Aziz, *ACS Energy Lett.* 2 (2017) 639–644.
- [45] Q. Chen, Y. Li, Y. Liu, P. Sun, Z. Yang, T. Xu, *ChemSusChem* 14 (2021) 1295–1301.
- [46] J.S. Steen, J.L. Nuismer, V. Eiva, A.E.T. Wiglema, N. Daub, J. Hjelm, E. Otten, *J. Am. Chem. Soc.* 144 (2022) 5051–5058.
- [47] J. S Tracy, E.S. Horst, V.A. Roytman, F.D. Toste, *Chem. Sci.* 13 (2022) 10806.
- [48] C. Zhang, Y. Qian, Y. Ding, L. Zhang, X. Guo, Y. Zhao, G. Yu, *Angew. Chem., Int. Ed.* 58 (2019) 7045–7050.
- [49] D. Xu, C. Zhang, Y. Zhen, Y. Zhao, Y. Li, *J. Power Sources* 495 (2021) 229819.